Available online at www.sciencedirect.com
ScienceDirect
Journal of Solid State Chemistry 180 (2007) 489–495
JOURNAL OF SOLID STATE CHEMISTRY
www.elsevier.com/locate/jssc

Template free fabrication of hollow hematite spheres via a one-pot polyoxometalate-assisted hydrolysis process

Baodong Mao[a], Zhenhui Kang[a], Enbo Wang[a,*], Chungui Tian[a], Zhiming Zhang[a], Chunlei Wang[a], Yanli Song[a], Meiye Li[b]

[a]*Institute of Polyoxometalate Chemistry, Department of Chemistry, Northeast Normal University, Changchun, Jilin 130024, PR China*
[b]*Changchun Institute of Applied Chemistry, Chinese Academy of Sciences, Jilin 130022, PR China*

Received 14 July 2006; received in revised form 2 November 2006; accepted 3 November 2006
Available online 11 November 2006

Abstract

Uniform hollow hematite (α-Fe_2O_3) spheres with diameter of about 600–700 nm and shell thickness lower than 100 nm are obtained by direct hydrothermal treatment of dilute $FeCl_3$ and tungstophosphoric acid $H_3PW_{12}O_{40}$ solution at 180 °C. The hollow spheres are composed of robust shells with small nanoparticles standing out of the surface and present a high-surface area and a weak ferromagnetic behavior at room temperature. The effect of concentration of $H_3PW_{12}O_{40}$, reaction time and temperature for the formation of the hollow spheres are investigated in series of experiments. The formation of the hollow spheres may be ascribed to a polyoxometalte-assisted forced hydrolysis and dissolution process.

Keywords: Hematite; Hollow spheres; One-pot synthesis; Nitrogen adsorption–desorption

1. Introduction

Recently fabrication of nanomaterials with desired morphologies has attracted more and more interests due to various shape-induced functions. Among the nanomaterials of different morphologies, hollow spheres of nanometer to micrometer dimensions attract much research interests recently because of their wide potential applications including controlled release capsules of various substances, artificial cells, catalysts, fillers, coatings and pigments [1–7]. The general approach for preparing such materials is based on the use of various templates including latex spheres, resin spheres, microemulsions, polymer micelles and block copolymers [8–16], by which hollow spheres of numerous materials have been successfully obtained. However, introduction of impurities to the products are usually inevitable in these template methods and the removing is usually time-consuming. So template-free synthesis methods for hollow spheres are of great interest by exploring the own chemical properties of the synthetic systems [17–20].

Among various inorganic materials, hematite (α-Fe_2O_3), a semiconductor with the band gap of 2.2 eV, is widely used in catalysts, pigments, sensors and as the raw material for the synthesis of magnetic γ-Fe_2O_3 [21–25]. Besides the conventional applications of hematite in these fields, improved catalysis property, gas sensitivity and electrochemical activity and photocatalytic activity have been reported in the hollow structured hematite particles including nanotubes [26–28], hollow nanowires [29] and hollow spheres [30–32]. However, the reported hollow hematite spheres are generally fabricated by using polystyrene spheres as template [30] or by surfactant-assisted solvothermal method [31,32]. Thus exploring simple and low cost methods for the synthesis of hollow hematite spheres is of great interest for its further large-scale applications in catalysts and encapsulation.

On the other hand, synthesis of hematite particles has been profoundly investigated and monodispersed particles with controlled shapes and sizes can be steadily prepared by the simple forced hydrolysis process of Fe^{3+} with or

*Corresponding author. Fax: +86 431 5098787.
E-mail address: wangenbo@public.cc.jl.cn (E. Wang).

0022-4596/$ - see front matter © 2006 Elsevier Inc. All rights reserved.
doi:10.1016/j.jssc.2006.11.005

without the addition of shape controllers, mainly inorganic anions, based on the selective adsorption and coordination chemistry in the solution system [21,33–35]. This is a mature process developed for decades that may have potential uses in template-free synthesis of uniform hollow nanostructures, such as nanotubes reported by Jia et al. [26] recently. And further exploration of this system may meet the need of large-scale synthesis of hematite hollow structures, in which polyoxometalates (POMs) may have potential uses owing to their widely studied coordination chemistry.

Polyoxometalates are one class of widely used inorganic metal-oxygen cluster compounds, especially as excellent catalysts owing to their unique electronic characteristics and structural robustness [36–40]. Recently, it was also introduced into the morphology-controlled fabrication of nanostructures and has become more and more remarkable in material synthesis field [41–47]. Especially, some recent work represented the utilization of the adsorption of POMs on nanoparticle surface for the preparation of Au@Ag [42], Au@Pd and Au@Pt [43] core-shell nanoparticles and carbon nanostrutures [45,46]. On the other hand, the coordination interaction of POMs and transition metal ions is another important property of polyoxometalates, based on which a lot of functional inorganic compounds have been synthesized [48–51]. And this may render the POMs more applications in the rational synthesis of nanomaterials.

In this paper, Keggin type POMs anion $PW_{12}O_{40}^{3-}$ is introduced to the forced hydrolysis process of Fe^{3+} as an assistant and uniform hollow hematite spheres are obtained by direct hydrothermal treatment. The as synthesized hollow spheres are composed of robust shells with small nanoparticles standing out of the surface and present a high-surface area and a weak ferromagnetic behavior at room temperature. Although the action mechanism of $PW_{12}O_{40}^{3-}$ in this procedure is still unclear, series of experiments showed that $PW_{12}O_{40}^{3-}$ played a key role in the formation of the hollow spheres.

2. Experimental section

All chemicals (analytical grade reagents) were purchased from Beijing chemicals Co. Ltd. and used as received without further purification. The hematite hollow spheres were fabricated by hydrothermal treatment of a mixture of dilute $FeCl_3$ and H_3PW_{12} solutions. In a typical synthesis, 0.20 mL of 1 M $FeCl_3$ aqueous solution and 0.40 mL of 0.01 M $H_3PW_{12}O_{40}$ aqueous solution were added into 9.40 mL distilled water with vigorous stirring to form a solution of 0.02 M $FeCl_3$ and 4×10^{-4} M $H_3PW_{12}O_{40}$. After stirring for a few minutes, the mixture was transferred into a Teflon-lined stainless-steel autoclave with a capacity of 15 mL. The autoclave was maintained at 180 °C for 8 h and then allowed to cool to room temperature naturally. The red precipitate was then separated by centrifugation, washed with distilled water and ethanol to remove the remained ions, and dried under vacuum at 70 °C for 24 h. The parameters that are essential for the formation of hollow spheres were also studied by varying concentration of $H_3PW_{12}O_{40}$, reaction time and temperature.

X-ray diffraction patterns were measured using a Rigaku D/max-IIB X-ray diffractometer at a scanning rate of 4°/min with 2θ ranging from 10° to 70°, using Cu $K\alpha$ radiation ($\lambda = 1.5418$ Å). The size and morphology of the hematite hollow spheres were characterized with transmission electron microscope (TEM, JEM-2010) at an acceleration voltage of 200 kV and field emission scanning electron microscopy (FESEM; XL30, FEG, FEI Company). The samples were dispersed in absolute ethanol and ultrasonicated before SEM and TEM observation. UV-vis absorption spectra were recorded using a 752 PC UV-vis spectrophotometer. The Fourier transform infrared (FTIR) absorption spectrum was obtained in the absorbance mode using a Bio-Rad FTS135 spectrophotometer. Nitrogen (N_2) adsorption–desorption isotherms were measured at liquid nitrogen temperature (77 K) using a Nova l000 analyzer. The sample was degassed for 6 h at 150 °C before the measurements. Surface areas were calculated by the Brunauer–Emmett–Teller (BET) method from the data in the P/P_0 region 0.05–0.35 and pore sizes by the Barrett–Joyner–Halenda (BJH) method at a relative pressure of 0.95(P/P_0). Magnetic measurements were carried out on a Quantum Design MPMS-XL5 SQUID magnetometer at room temperature with the field sweeping from −10,000 to 10,000 Oe.

3. Results and discussion

Scanning electron microscopy (SEM) is employed to observe the size and morphology of the hematite hollow spheres prepared in standard condition (0.02 M $FeCl_3$ and 4×10^{-4} M $H_3PW_{12}O_{40}$, 180 °C for 8 h) as shown in Fig. 1. Fig. 1a shows the overall morphology of the sample, indicating that it consists of relatively uniform microspheres with diameter of 600–700 nm. Fig. 1b is a higher magnification image. Magnified view of a single sphere in Fig. 1c indicates that the spheres are composed of continuous robust shells with small nanoparticles sticking out. Some of the hollow spheres are broken, which enables the direct observation of the shell structure. The shell thickness is smaller than 100 nm calculated from Fig. 1d.

The morphology and structure of the hematite hollow spheres are further studied with TEM and SAED. Fig. 2 shows typical characterizations of the structure and phase of the product. Fig. 2a shows the typical TEM image indicating the uniformity and hollow structure of the sample. Although the hollow spheres have small nanoparticles standing on the outer surface, most of them still have continuous but coarse shells as shown in both TEM and SEM images. The selected area electron diffraction (SAED) pattern in Fig. 2b shows that the spheres behave as a polycrystalline phase.

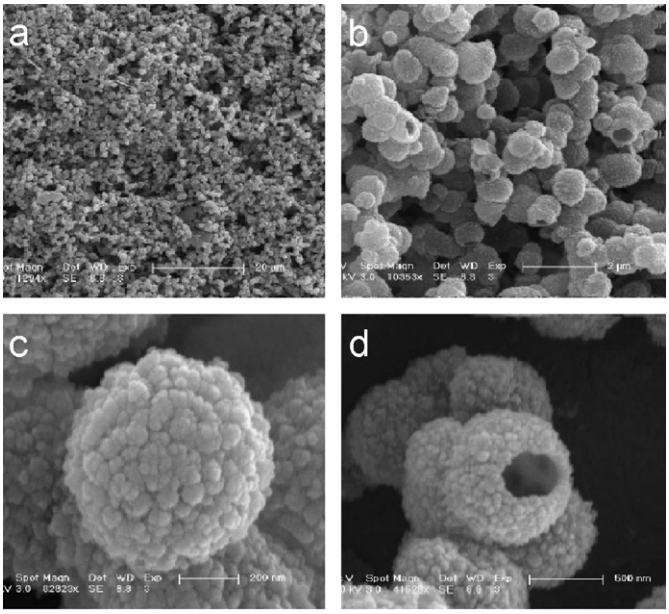

Fig. 1. Typical SEM images of the hollow hematite spheres.

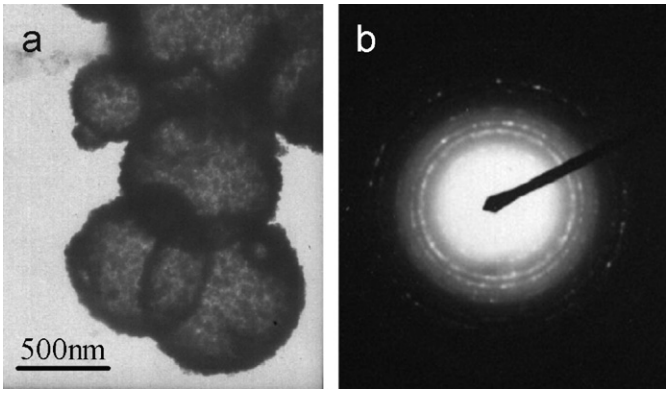

Fig. 2. Typical TEM image and SAED pattern of the hollow hematite spheres.

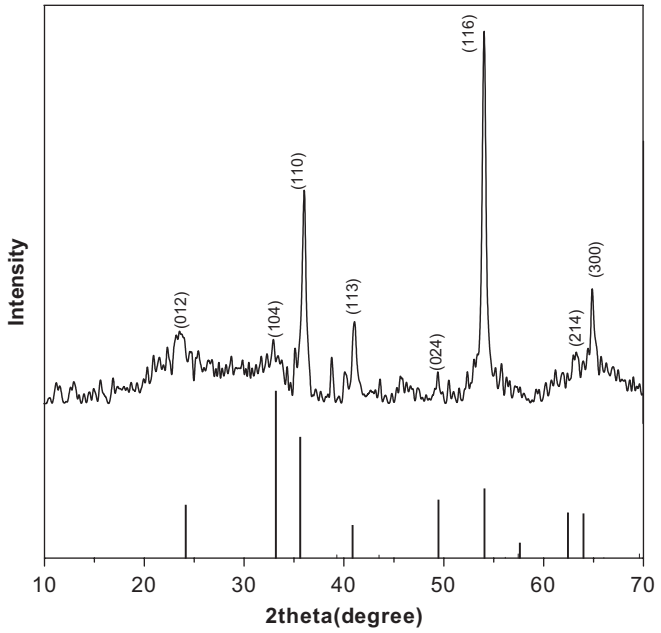

Fig. 3. XRD pattern of the hollow hematite spheres and standard XRD spectrum of hematite.

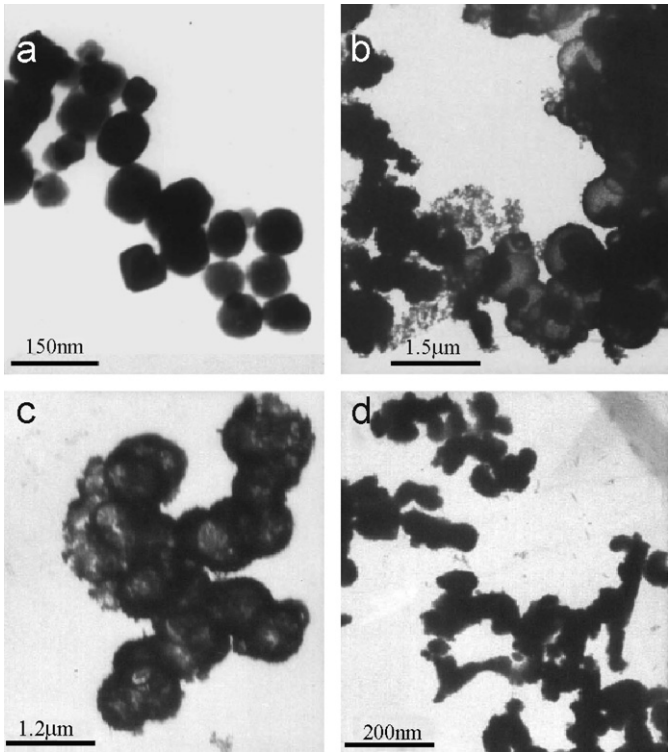

Fig. 4. Products prepared with 0.02 M Fe^{3+} and different concentrations of $H_3PW_{12}O_{40}$: (a) 0, (b) 1×10^{-4} M, (c) 8×10^{-4} M and (d) 20 $\times 10^{-4}$ M.

Fig. 3 shows typical XRD pattern of the hollow hematite spheres. All peaks in the XRD pattern can be indexed as α-Fe_2O_3 (JCPDF no. 33-664). No peaks for impurities are detected. Broadening of the reflection peaks was observed in their corresponding XRD patterns, for that the shells of the hollow spheres have small nanoparticles standing on the outer surface as observed in TEM and SEM.

Series of experiments performed by varying concentration of $H_3PW_{12}O_{40}$ with other parameters unchanged suggested that concentration of the polyoxometalate $H_3PW_{12}O_{40}$ played a key role in the formation of the hollow spheres. It was found that the concentration of $H_3PW_{12}O_{40}$ should be confined in a small range around 4×10^{-4} M. Without $H_3PW_{12}O_{40}$, small polyhedral nanoparticles with diameter of ~60 nm were obtained as shown in Fig. 4a. When the concentration was below 4×10^{-4} M, solid and hollow spheres usually coexisted in the sample and the shell thickness of the hollow spheres is not uniform (Fig. 3b, 13.1×10^{-4} M). The best result was observed with 0.02 M $FeCl_3$ and 4×10^{-4} M $H_3PW_{12}O_{40}$ reacting for 8 h, showing clear and fine hollow structure as shown in Figs. 1 and 2. With the increase of the concentration of

$H_3PW_{12}O_{40}$, both hollow spheres with thick and rough shells and destroyed spheres appeared in the product (Fig. 3c, 83.8×10^{-4} M). Further increase of the concentration to 2×10^{-3} M destroys the environment for the formation of hollow spheres and only irregular particles are obtained (Fig. 3d).

For a clear view of the role of $PW_{12}O_{40}^{3-}$ in the formation process of the hollow spheres, series of control experiments were carried out and a phase evolution was observed depending on the reaction time and temperature. Fig. 5 shows typical TEM images of the products obtained at 180 °C for different reaction time: (a) 15 min, (b) 2 h, and (c) 48h, and at different temperature for 8 h: (d) 100 °C, (e) 140 °C, (f) 200 °C with 0.02 M Fe^{3+} and 4×10^{-4} M $H_3PW_{12}O_{40}$ A short reaction time (15 min) resulted in the formation of immature particles and a few of solid spheres (Fig. 4a), which may be the precursor of hollow spheres. A mixture of solid and hollow spheres was formed with the elongation of the reaction time to 2 h (Fig. 4b). Product composed of perfect hollow spheres was obtained after reacting for 8 h as mentioned above (Fig. 1 and 2). The hollow spheres obtained after reacting for 48 h show thick and coarse shells (Fig. 4c) different from the 8 h sample.

The growth control of hematite particles by the adsorption of phosphate ions and other inorganic anions has been extensively studied in the hydrolysis process [21,26,33–35]. Recently, Jia et al reported a rational synthesis of single-crystalline hematite nanotubes by a coordination-assisted dissolution process with $FeCl_3$ and $NH_4H_2PO_4$, in which the formation of a tubular structure is attributed to the selective adsorption of phosphate ions on the surfaces of hematite particles and their ability to coordinate with ferric ions. The formation mechanism is clearly demonstrated with the selected etching of the nanospindle precursor by $H_2PO_4^-$ [26]. On the other hand, coordination chemistry of POMs and transition metal ions has been researched for many years, based on which a lot of functional inorganic compounds have been synthesized [36,45–48]. And as mentioned above, some recent work represented the utilization of the adsorption of POMs on nanoparticle surface, for example, Keggin ion-mediated synthesis of aqueous phase-pure Au@Ag [42], Au@Pd and Au@Pt [43] core-shell nanoparticles, stabilizing platinum nanoparticles with POMs based on their physical presence and electrostatic properties [45] and adsorbing POMs on carbon surfaces to obtain highly monodispersed colloidal carbon nanoparticles [46]. Our group also reported the POMs assisted growth of carbon nanotubes and nanobelts from amorphous carbon [47].

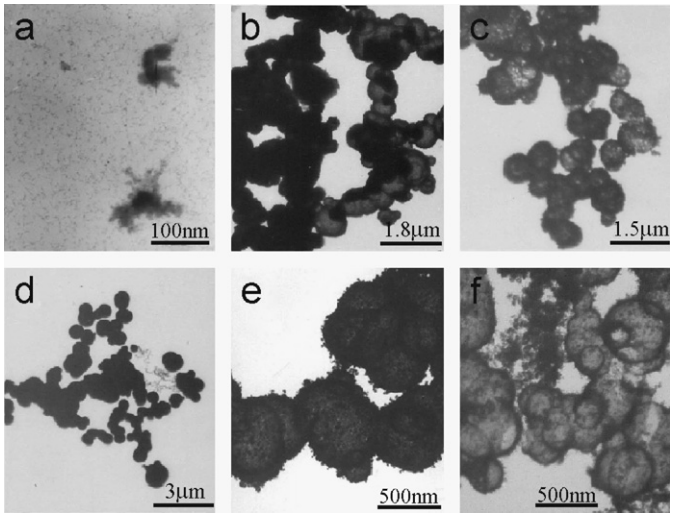

Fig. 5. Hematite spheres prepared at 180 °C for different reaction time: (a) 15 min, (b) 2 h and (c) 48 h; and at different temperature for 8 h: (d) 100 °C, (e) 140 °C, (f) 200 °C with 0.02 M Fe^{3+} and 4×10^{-4} M $H_3PW_{12}O_{40}$.

Formation of the hollow hematite spheres may be also attributed to the selective adsorption and the coordination chemistry of the POMs. A similar dissolution process is also observed in our experiments. But the partly etched spheres were hardly found in our process. A possible reason for this difference may be that the POMs-assisted dissolution process is temperature dependent, e.g. it can only take place at high temperature. The further temperature-dependent study suggested this point. The product obtained at 100 °C is composed of complete solid spheres (Fig. 5d). The hollow spheres of 140 °C have a thicker and coarser shell than that of 180 °C as shown in Fig. 5e. Further increase of temperature to 200 °C shows similar results with 180 °C (Fig. 5f). The hydrolysis process of pure 0.02 M $FeCl_3$ solution forms spherical particles of 100–200 nm without any other shape controller, spindle-like particles with PO_4^{3-} or $H_2PO_4^-$ [33–35]. It sill forms spherical particles with POMs as an assistant (Fig. 5d). So Jia et al obtained hematite nanotubes from the spindle-like precursor with $FeCl_3$ and $NH_4H_2PO_4$ reacting at 220 °C [26] and the product in the present work is hollow spheres from the sphere-like precursor with $FeCl_3$ and $H_3PW_{12}O_{40}$ at 180 °C.

Further UV-vis absorbance and FTIR spectrum investigation of the filtrate after separation of the hematite spheres indicates the existence of $PW_{12}O_{40}^{3-}$ and its stability during hydrothermal treatment. Fig. 6 shows the UV-vis absorbance spectra of the filtrate. The characteristic band at 254 nm is ascribed to the oxygen → tungsten charge-transfer (CT) transition of polyoxometalates. Fig. 7 is FTIR spectrum of the precipitate from the filtrate after hydrothermal treatment. The absorption bands at 1080, 983, 888, 805 cm^{-1} are the characteristic bands of $PW_{12}O_{40}^{3-}$, which should be ascribed to the vibration modes of ν (W = Ot), ν (P–Oa), ν (W–Ob–W) and (W–Oc–W), respectively (where Oa is the oxygen in P–O tetrahedron, Ot is the terminal oxygen, Ob is the bridging oxygen of two octahedra sharing a corner, and Oc is the bridging oxygen of two octahedra sharing an edge) [36]. This shows that the original framework of $PW_{12}O_{40}^{3-}$ is not destroyed after hydrothermal treatment.

As both a coarse outer surface and a robust shell are observed in the hollow spheres, some interesting properties might be expected. Fig. 6 shows the N_2

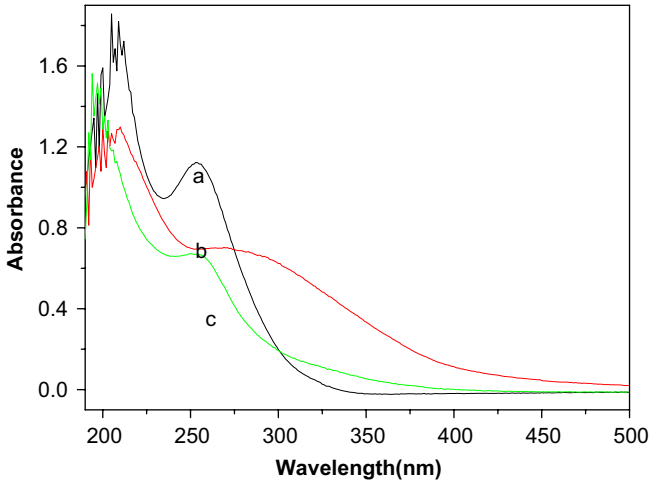

Fig. 6. UV-vis absorbance spectra of $H_3PW_{12}O_{40}$ (a), the $H_3PW_{12}O_{40}$ and $FeCl_3$ solution before (b) and after (c) hydrothermal treatment (with $[H_3PW_{12}O_{40}] = 4 \times 10^{-6}$ M and length of absorption cell $L = 1$ cm).

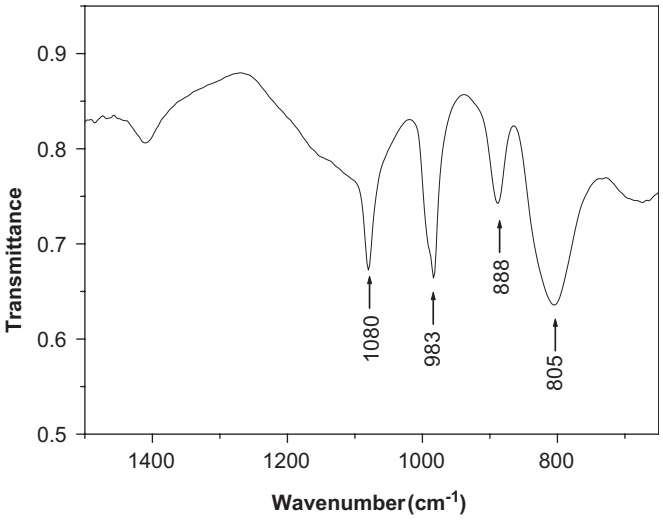

Fig. 7. FTIR spectrum of the precipitate from the solution after hydrothermal treatment.

adsorption–desorption isotherm and pore size distribution of the hollow hematite spheres. The Brunauer–Emmett–Teller (BET) surface area is 135.77 m^2/g calculated from the data in the P/P_0 region 0.05–0.35, which is higher than that (50 m^2/g) of the α-Fe_2O_3 nanoparticles prepared by the homogeneous precipitation method [52]. The hollow spheres have pores mainly focusing in the range of 1.5–5 nm, indicating the coarse structure of the shell (Fig. 8).

Recent studies indicate that magnetic properties of the hematite nanostructures strongly depend on their shape and structure [53,54]. Normally, bulk hematite has the Morin transition from the low-temperature antiferromagnetic phase to a canted ferromagnetic phase at 260 K besides the well-known Néel temperature, $T_N = 961$ K [55,56]. However, magnetic behavior of the hollow hematite spheres is completely different from bulk hematite

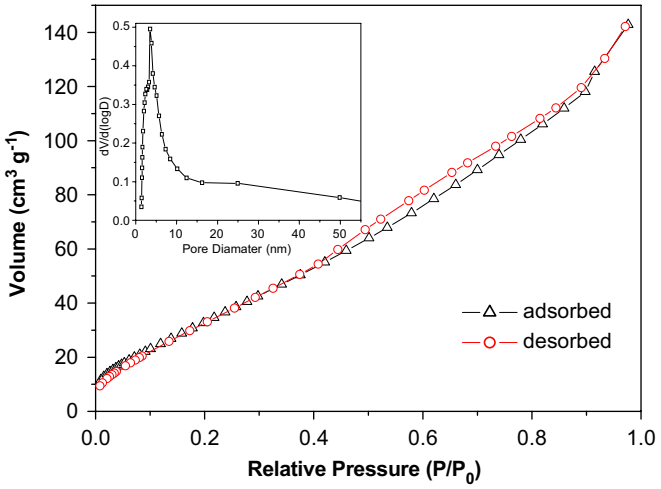

Fig. 8. Nitrogen adsorption-desorption isotherm of the hematite hollow spheres. The inset is its BJH pore-size distribution curve.

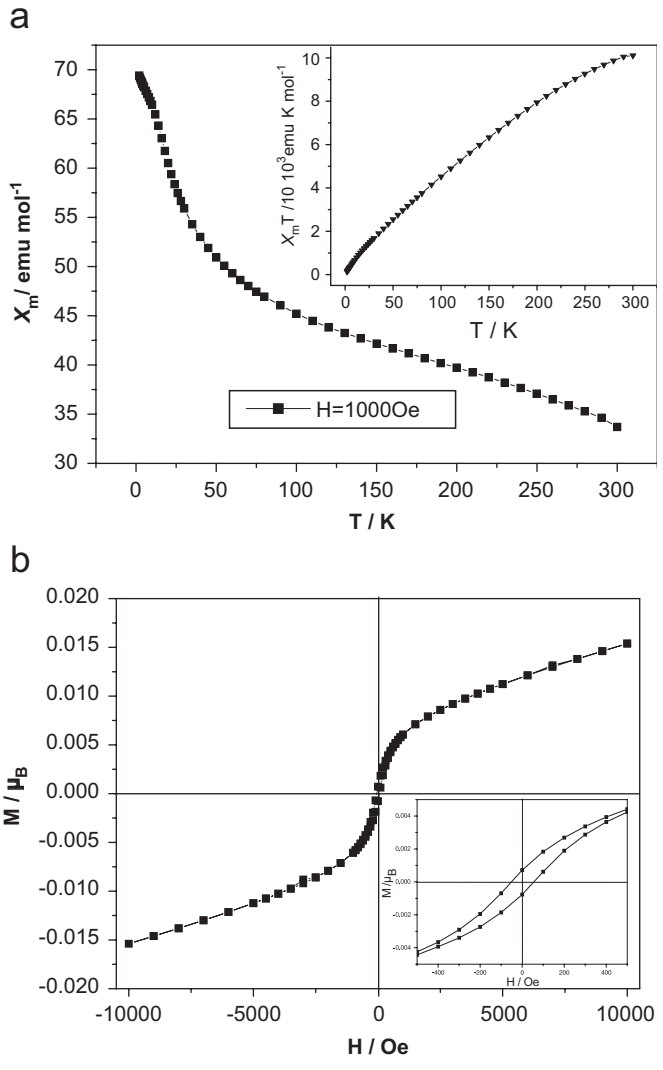

Fig. 9. Magnetic measurements for the hollow hematite spheres: (a) temperature dependence of magnetic susceptibility (applied field of 1000 Oe). The inset is the plot of $\chi_m T$ vs. T. (b) Hysteresis loop curve measured at 300 K. The inset shows a magnified view.

and most reported hematite nanostructures. As shown in Fig. 9a, the temperature dependence plot of magnetic susceptibility measured in an applied field of 1000 Oe shows a constant increase in χ_m and no maximum down to 2 K with no Morin transition. The inset is the plot of $\chi_m T$ vs. T. Similar phenomena has only been observed recently in mesoporous α-Fe_2O_3 with disordered walls [57] and small α-Fe_2O_3 nanotubes [58], in which the abnormality was assigned to the presence of small crystalline particles in a few regions of the samples that provide sufficient spin interactions occurring along the walls to align the neighboring spins. Here, it may be ascribed to the mesoporous structure of the hollow hematite spheres that resulted in the abnormal magnetic behavior. Fig. 9b shows the magnetic hysteresis loop curve of the hollow hematite spheres measured at 300 K. It shows typical weak ferromagnetic behavior of hematite, indicating the value of coercivity 55.4 Oe.

The as-obtained hollow hematite spheres with high surface area and no organic group modifying on the surface may have potential applications for the design of novel complex structures, as carriers in biomagnetic sensors, nanomedicine, encapsulation of various guest molecules and catalysis and as the raw material for the synthesis of magnetic γ-Fe_2O_3 [26–32]. Magnetic iron oxides are still the most important and safest materials for drug delivery and biomagnetic sensors [21,22]. This convenient and low-cost method may meet the need of large-scale synthesis of hematite hollow spheres for further large-scale applications in catalysts and encapsulation.

4. Conclusions

In summary, uniform hollow hematite spheres were successfully synthesized by a simple polyoxometalate-assisted hydrolysis process of Fe^{3+} in hydrothermal condition. The hollow spheres with diameters of 600–700 nm are composed of continuous robust shells with small nanoparticles sticking out of the surface. A high surface area and weak ferromagnetic behavior are observed in the product. The polyoxometalate anion $PW_{12}O_{40}^{3-}$ played a key role in the formation of the hollow spheres. This convenient and low-cost method provides a rational synthetic alternative for the preparation of hollow hematite spheres, which may be applied to hollow nanostuctures of other oxides and the further work is still on going.

Acknowledgements

This work was financially supported by the National Natural Science Foundation of China (20371011).

References

[1] F. Caruso, R.A. Caruso, H. Möhwald, Science 282 (1998) 1111.
[2] F. Caruso, Chem. Eur. J. 6 (2000) 413.
[3] F. Caruso, Adv. Mater. 13 (2001) 11.
[4] W. Schärtl, Adv. Mater. 12 (2000) 1899.
[5] Z. Zhong, Y. Yin, B. Gates, Y. Yia, Adv. Mater. 12 (2000) 206.
[6] C.E. Fowler, D. Khushalani, S. Mann, J. Mater. Chem. 11 (2001) 1968.
[7] A.B. Bourlinos, M.A. Karakassides, K. Petridis, Chem. Commun. (2001) 1518.
[8] I. Radtchenko, G.B. Sukhorukov, N. Gaponik, A. Kornowski, A.L. Rogach, Adv. Mater. 13 (2001) 463.
[9] P.V. Braun, S.I. Stupp, Mater. Res. Bull. 34 (1999) 463.
[10] H.T. Schmidt, A.E. Ostafin, Adv. Mater. 14 (2002) 532.
[11] T. Liu, Y. Xie, B. Chu, Langmuir 16 (2000) 9015.
[12] P.J. Brusinsma, A.Y. Kim, J. Liu, S. Baskaran, Chem. Mater. 9 (1997) 2507.
[13] L. Qi, J. Li, J. Ma, Adv. Mater. 14 (2002) 300.
[14] E. Prouzet, F. Cot, C. Boissiere, P.J. Kooyman, A. Larbot, J. Mater. Chem. 12 (2002) 1553.
[15] N.A. Dhas, K.S. Suslick, J. Am. Chem. Soc. 127 (2005) 2368.
[16] M. Yang, J. Ma, C. Zhang, Z. Yang, Y. Lu, Angew. Chem. Int. Ed. 44 (2005) 6727.
[17] Y.G. Zhang, S.T. Wang, X. Wang, Y.T. Qian, Z.D. Zhang, J. Nanosci. Nanotech. 6 (2006) 1423.
[18] X. Li, Y. Xiong, Z. Li, Y. Xie, Inorg. Chem. 45 (2006) 3493.
[19] E.S. Kang, M. Takahashi, Y. Tokuda, T. Yoko, Langmuir 22 (2006) 5220.
[20] H.L. Zhu, K.H. Yao, H. Zhang, D.R. Yang, J. Phys. Chem. B 109 (2005) 20676.
[21] R.M. Cornell, U. Schwertmann, The Iron Oxides: Structure, Properties, Reactions, Occurrences, Uses, Wiley-VCH Verlag GmbH & Co. KGaA, Weinheim, 2003.
[22] M.A. Willard, L.K. Kuriharal, E.E. Carpenter, S. Calvin, V.G. Harris, Int. Mater. Rev. 49 (2004) 125.
[23] L. Huo, W. Li, L. Lu, H. Cui, S. Xi, J. Wang, B. Zhao, Y. Shen, Z. Lu, Chem. Mater. 12 (2000) 790.
[24] W.T. Dong, C.S. Zhu, J. Mater. Chem. 12 (2002) 1676.
[25] R.H. Kodama, S.A. Makholoufand, A.E. Berkowitz, Phys. Rev. Lett. 79 (1997) 1393.
[26] C.J. Jia, L.D. Sun, Z.G. Yan, L.P. You, F. Luo, X.D. Han, Y.C. Pang, Z. Zhang, C.H. Yan, Angew. Chem. Int. Edn. 44 (2005) 4328.
[27] J. Chen, L. Xu, W.Y. Li, X.L. Gou, Adv. Mater. 17 (2005) 582.
[28] L. Suber, P. Imperatori, G. Ausanio, F. Fabbri, H. Hofmeister, J. Phys. Chem. B. 109 (2005) 7103.
[29] Y.J. Xiong, Z.Q. Li, X.X. Li, B. Hu, Y. Xie, Inorganic Chemistry 43 (2004) 6541.
[30] H. Shiho, N. Kawahashi, J. Colloid Interf. Sci. 226 (2000) 91.
[31] D.H. Chen, D.R. Chen, X.L. Jiao, Y.T. Zhao, J. Mater. Chem. 13 (2003) 2266.
[32] S.Y. Lian, E.B. Wang, L. Gao, D. Wu, Y.L. Song, L. Xu, Mater Res. Bull. 41 (2006) 1192.
[33] M. Ozaki, S. Kratohvil, E. Matijevic, J. Colloid Interface Sci. 102 (1984) 146.
[34] T. Sugimoto, A. Muramatsu, K. Sakata, D.J. Shindo, J. Colloid Interface Sci. 158 (1993) 420.
[35] N. Kallay, I. Fischer, E. Matijevic, ColloidsSurf 13 (1985) 145.
[36] M.T. Pope, A. Müller (Eds.), Polyoxometalate Chemistry, Kluwer, Dordrecht, The Netherlands, 2001.
[37] I.V. Kozhevnikov, Chem. Rev. 98 (1998) 171.
[38] A.M. Khenkin, L. Weiner, R. Neumann, J. Am. Chem. Soc. 127 (2005) 9988.
[39] Z.H. Peng, Angew. Chem. Int. Ed. 43 (2004) 930.
[40] L. Gao, E.B. Wang, Z.H. Kang, Y.L. Song, B.D. Mao, L. Xu, J. Phys. Chem. B 109 (2005) 16587.
[41] P. Garrigue, M. Delville, C. Labrugére, E. Cloutet, P.J. Kulesza, J.P. Morand, A. Kuhn, Chem. Mater. 16 (2004) 2984.
[42] S. Mandal, P.R. Selvakannan, R. Pasricha, M. Sastry, J. Am. Chem. Soc. 125 (2003) 8440.
[43] S. Mandal, A.B. Mandale, M. Sastry, J. Mater. Chem. 14 (2004) 2868.

[44] J. Kim, L. Lee, B.K. Niece, J.X. Wang, A.A. Gewirth, J. Phys. Chem. B 108 (2004) 7927.
[45] P.J. Kulesza, M. Chojak, K. Karnicka, K. Miecznikowski, B. Palys, A. Lewera, A. Wieckowski, Chem. Mater. 16 (2004) 4128.
[46] P. Garrigue, M.H. Delville, C. Labrugere, E. Cloutet, P.J. Kulesza, J.P. Morand, A. Kuhn, Chem. Mater. 16 (2004) 2984.
[47] Z.H. Kang, E.B. Wang, B.D. Mao, Z.M. Su, L. Gao, S.Y. Lian, L. Xu, J. Am. Chem. Soc. 127 (2005) 6534.
[48] P.Q. Zheng, Y.P. Ren, L.S. Long, R.B. Huang, L.S. Zheng, Inorg. Chem. 44 (2005) 1190.
[49] R.C. Howell, F.G. Perez, S. Jain, W.D. Horrocks, J.A. Rheingold, L.C. Francesconi, Angew. Chem. Int. Ed. 40 (2001) 4031.
[50] L.H. Bi, U. Kortz, B. Keita, L. Nadjo, H. Borrmann, Inorg. Chem. 43 (2004) 8367.
[51] Z.M. Zhang, Y.G. Li, E.B. Wang, X.L. Wang, C. Qin, H.Y. An, Inorg. Chem. 45 (2006) 4313.
[52] J. Qiu, R. Yang, M. Li, N. Jiang, Mater. Res. Bull. 40 (2005) 1968.
[53] M. Cao, T. Liu, S. Gao, G. Sun, X. Wu, C. Hu, Z.L. Wang, Angew. Chem. Int. Ed. 44 (2005) 4197.
[54] T.P. Raming, A.J.A. Winnubst, C.M. van Kats, A.P. Philipse, J. Colloid Interface Sci. 249 (2002) 346.
[55] F. Gronvold, E.J. Samuelsen, J. Phys. Chem. Solids 36 (1975) 249.
[56] F.J. Morin, Phys. Rev. 78 (1950) 819.
[57] F. Jiao, A. Harrison, J.C. Jumas, A.V. Chadwick, W. Kockelmann, P.G. Bruce, J. Am. Chem. Soc. 128 (2006) 5468.
[58] L. Liu, H.Z. Kou, W.L. Mo, H.J. Liu, Y.Q. Wang, J. Phys. Chem. B. 110 (2006) 15218.